Effects of implantation temperature and annealing on structural evolution and migration of Se into glassy carbon

S.A. Adeojo [a, b, *], J.B. Malherbe [a], A. Azarov [c], O.S. Odutemowo [a], E. Njoroge [a, d], H.A.A. Abdelbagi [a], S. Mpelane [e], T.T. Hlatshwayo [a]

[a] *Physics Department, University of Pretoria, Pretoria, South Africa.*
[b] *Department of Physics and Engineering Physics, Obafemi Awolowo University, Ile-Ife, Nigeria.*
[c] *Department of Physics, Centre for Materials Science and Nanotechnology, University of Oslo, N-0316 Oslo, Norway.*
[d] *ENGAGE, University of Pretoria, Pretoria, South Africa.*
[e] *Analytical Facility, University of Johannesburg, South Africa.*

Abstract

The use of glassy carbon (GC) as a future nuclear waste storage material depends on its capability to retain all radioactive fission products found in spent nuclear fuels. Selenium (^{79}Se) is found in trace amounts in uranium ores, spent, and reprocessed nuclear fuel. This work investigates the effects of implantation temperature and annealing on the structural evolution and migration of Se implanted GC. To achieve these objectives, 150 keV Se^+ was implanted into GC samples separately at room temperature (RT) and 200ºC to a fluence of 1×10^{16} cm^{-2}. Some of the as-implanted samples were annealed at 1000, 1100 and 1200ºC for 5h and characterized by transmission electron microscopy (TEM), Raman spectroscopy, and secondary ion mass spectrometry (SIMS). Both TEM and Raman spectroscopy showed that implantation caused defects in the GC structures, with more defects in the RT as-implanted sample. Annealing caused the healing of both sample types but retained some radiation damage. No migration of Se atoms was observed in the RT and 200ºC as-implanted samples. However, a different migration behaviour was seen after annealing the RT and 200ºC samples up to 1200 ºC, attributed to the trapping and de-trapping of Se atoms in different amounts of defect induced by implantation.

Corresponding Author: Adeojo S.A.
Tel. Number: +27719153351
Email address: u19288124@tuks.co.za (Adeojo S.A.)

Graphical abstract

The figure below shows the influence of annealing on the migration behaviour of glassy carbon samples after implantation with 150 keV Se ions (fluence of 1×10^{16} cm^{-2}) at room temperature (RT) and 200 °C. The different migration patterns as observed in the RT and 200 °C samples after annealing, can be attributed to the trapping and de-trapping of Se atoms in different amounts of defect induced by implantation. The magnitude of defect induced at implantation are shown in the Raman and TEM images. Both Raman and TEM techniques confirms that the RT implanted sample is more damaged than the 200 °C implanted sample which justifies the different migration behaviour.

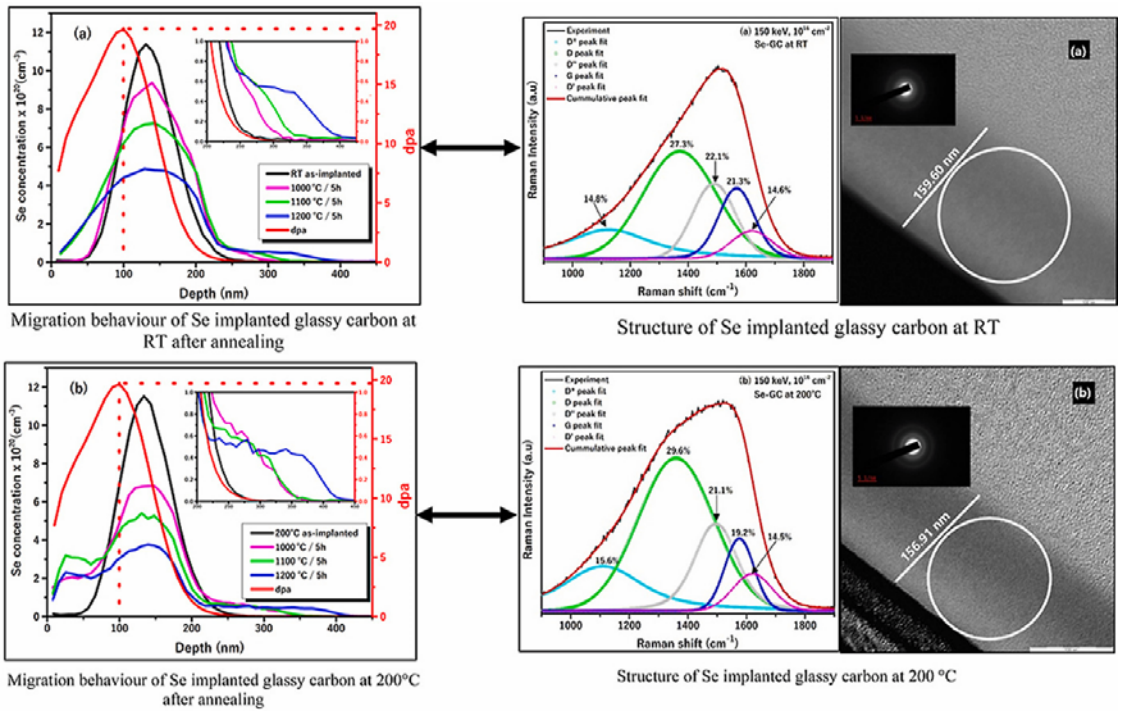

Keywords: TEM; SIMS; Raman, Implantation Defect; Trapping; De-trapping

1. Introduction

The management of high-level nuclear waste has been one of the major issues limiting the acceptance of nuclear energy as an alternative form of energy. High-level nuclear wastes (HLW) generated during the operation of a nuclear reactor are typically stored in specially designed storage pools. These wastes are allowed to cool and decay in the pool for some years and then transferred to dry casks for long-term storage. The materials for fabricating dry casks are mainly susceptible to degradation due to ageing [1], and as a result, the leakage of

radioactive material into the environment is possible. As there is currently limited operational permanent geological repositories to contain and dispose of high-level nuclear wastes, dry casks of longer lifespan could be in high demand in the nearest future. Therefore, the improvement and performance of the materials used to manufacture dry storage devices are vital. Previous studies on the migration behaviour of fission products in glassy carbon have shown that glassy carbon can serve as an alternative material to be considered for the dry cask needed for nuclear waste management [2–11].

Glassy carbon (GC) is a synthetic allotrope of carbon that combines glassy and ceramic properties with those of graphite. Heating organic resins produce glassy carbon at higher temperatures in the range of 900 – 3000 °C in an inert atmosphere. The structure of glassy carbon has been a major research interest since it was first fabricated in the 1960s. Recent investigations by Harris [12,13] using a High resolution transmission electron microscopy (HRTEM) suggest that glassy carbon has a fullerene-like structure. The fullerene-like property of glassy carbon is responsible for its remarkable properties, including superior hardness and strength, low reactivity, high-temperature stability [14], biocompatibility, resistance to chemical attacks and radiation, and impermeability by liquids and gases [15].

Selenium (Se) is a non-metallic element that occurs naturally in trace quantities in aquatic, atmospheric, and terrestrial ecosystems. Among the various selenium isotopes, ^{79}Se is the only radioisotope that falls into the seven most long-lived radioactive fission products. This isotope of selenium, ^{79}Se can be found in trace amounts (~0.0487 % yield) [16] in uranium ores, spent, and reprocessed nuclear fuel. The physical half-life of ^{79}Se, about $3.77(\pm0.19) \times 10^5$ years [17], makes it applicable in evaluating the long-term radiological impact of geological repositories [18]. The release of ^{79}Se into different environmental media would pose a health hazard from the β-particles released during its radioactivity. Selenium toxicity can cause cancer, especially when swallowed or absorbed into the body at a dose higher than 400 μg per day [19].

The applicability of glassy carbon as a material for nuclear waste containment would require it to be highly resistant to radiation damage produced from the high-level radioactive nuclear waste. It should also be a reliable diffusion barrier for fission product elements present in nuclear waste. Some studies have shown that ion implantation is useful in understanding the effect of radiation damage on the glassy carbon structure [3–8,20–23]. Similarly, these studies have shown that post-implantation annealing caused the migration of the implanted impurities in glassy carbon. For example, in our previous study, we found that radiation damage was induced in GC implanted with Se ions at room temperature (RT) [8]. We further reported that

sequential isochronal annealing resulted in Se's diffusion towards the GC surface. Still, the GC structure does not recover after annealing at 1200 ºC [8]. Typically, the radioactivity of nuclear waste generates heat and can abruptly lead to the high temperature of the nuclear waste storage system [2]. To simulate the radiation conditions of the proposed GC (as nuclear waste storage device) would be exposed to, the material was implanted with a typical radioactive fission element, selenium (Se) at RT and at a high temperature of 200 ºC, both to a fluence of 1×10^{16} ions/cm^2. The idea was to compare the radiation damage induced in the GC substrates due to Se implantation at RT and elevated temperature. The annealing of radiation damage together with the migration behaviour of Se in GC is also investigated in this study.

2. Experimental

The starting material was commercially available SIGRADUR®G glassy carbon (GC) samples purchased from Hochtemperatur-Werkstoffe GmbH, Germany. Each glassy carbon strip was of a rectangular size of 50 mm × 10 mm × 2 mm. According to the manufacturer, the SIGRADUR®G grade has a density of 1.42 g/cm^3, Young's modulus of 35 GPa, thermal conductivity of 6.3 Wm^{-1}K^{-1}, flexural strength of 260 MPa, compressive strength of 480 MPa, and a maximum service temperature of 3273 K [24]. Each as-received glassy carbon sample was polished on one side, and the unpolished surface was marked into ten (10) rectangular sections to enable easy separation. The glassy carbon samples were cleaned sequentially in an ultrasonic bath with a soap solution, deionised water, and methanol and dried using nitrogen gas. The polished surface of the cleaned GC samples was implanted with 150 keV Se ions to a fluence of 1×10^{16} cm^{-2} at RT and 200 ºC. The Se beam was raster scanned across each GC strip to ensure uniform implantation. The implantation flux was maintained at 10^{13} cm^{-2}s^{-1} to prevent the annealing of the radiation damage introduced into the GC during implantation. After implantation, the samples were cut into more petite strips through the marks on the unpolished surfaces.

The as-implanted samples were characterised by transmission electron microscopy (TEM). TEM lamellas were prepared by the Focused Ion Beam (FIB) technique using a FEI Helios Nanolab 650 FIB. The thinning of the samples was performed by successive 30 keV and 5 keV Ga ions. The final polishing was done at 2 keV and 500 eV, which produced near damage-free TEM foils. TEM analysis was then performed using a JEOL JEM 2100 LaB6 transmission electron microscope operating at 200 kV acceleration voltage.

The glassy carbon structure before implantation, after implantation, and annealing were investigated by Raman spectroscopy. The argon excitation laser line of 532 nm wavelength

was employed for the Raman measurements. The 50 × objective lens was used to acquire the spectra with the laser power set at 0.82 mW. The spectrometer system was operated in the double subtractive mode to reject the Rayleigh scattering and disperse the Raman scattering onto a liquid nitrogen-cooled Symphony CCD detector. A Voigt function was fitted onto the Raman data to obtain information such as the full width at half maximum (FWHM) of the G band, peak positions, and the intensities. A Voigt function is a convolution product between a Lorentzian function and a Gaussian function as given by equation (1) below:

$$y = y_0 + A\frac{2\ln 2}{\pi^{3/2}}\frac{\omega_L}{\omega_G^2}\int_{-\infty}^{\infty}\frac{e^{-t^2}}{(\sqrt{\ln 2}\frac{\omega_L}{\omega_G})^2+(\sqrt{4\ln 2}\frac{x-x_c}{\omega_G}-t)^2}\,dt \qquad (1)$$

For each Voigt profile, y_0 represents the offset value, x_c is the center of the profile, A represents the area under the profile, ω_G = Gaussian FWHM, ω_L = Lorentzian FWHM. A constant (minimum) baseline mode was chosen for each Raman fittings.

The migration behaviour of selenium and the annealing of radiation damage was investigated by annealing some of the implanted samples isochronally (in vacuum) at 1000, 1100, and 1200 ºC for 5 h. The details of the annealing set-ups and procedures can be found in [25]. The depth profiles of the as-implanted glassy carbon samples before and after annealing were measured by secondary ion mass spectrometry (SIMS) with a Cameca IMS 7f microanalyser. For each measurement, a primary beam of 10 keV O^{2+} ions was raster scanned across the sample area of 150 × 150 μm^2. The intensity-concentration calibration was achieved with the as-implanted samples as reference. Finally, the depth conversion of the recorded profiles was performed by measuring the sputtered crater depth with a DEKTAK 8 stylus profilometer and assuming a constant erosion rate with time.

3. Results and Discussion

One of the important reasons for carrying out "Stopping Range of Ions in Matter" (SRIM) simulation was to estimate the amount of radiation damage created in the substrate due to ion implantation. Typically, the average number of displacements of atoms from a lattice during implantation is used to estimate the radiation damage induced in the material. The simulation of the depth profile of 150 keV Se ions implanted in glassy carbon was carried out using SRIM in the full cascade mode. The density of glassy carbon was assumed to be 1.42 g/cm^3 ~ 7.12 × 10^{22} atoms/cm^3. The damage event in SRIM is processed as vacancy/ion (in Angstrom unit), which can be converted to displacement per atom (dpa) at a required

dose/fluence. The vacancies/ion (obtained from SRIM) was converted into displacement per atom (dpa) using equation (2) below [6]:

$$\text{dpa} = \frac{\left({}^{V_{ac}}/_{ion(\text{Å})\times 10^{8}}\right)\times \varphi\left(\frac{ion}{cm^{2}}\right)}{\rho_{GC}\left(\frac{atoms}{cm^{3}}\right)} \quad (2)$$

${}^{V_{ac}}/_{ion(\text{Å})}$ is the vacancy per ion in Angstrom units, 10^8 is a conversion factor from Angstrom (Å) to a centimetre (cm), φ is the Se ion fluence (1×10^{16} ions/cm^2), and ρ_{GC} is the atomic density of the GC (7.12×10^{22} atoms/cm^3).

The SIMS depth profiles of Se implanted into GC at room temperature and 200 °C, the simulated ion distribution (from SRIM), and damage profile in dpa (from SRIM) are shown in Figure 1. An Edgeworth function was fitted onto the SIMS spectra, and the first four moments of the distribution were obtained and compared with the SRIM value, as shown in Table 1. The experimental projected range (R_p) was estimated at approximately 130 nm in the RT and 200 °C as-implanted Se profiles. The as-implanted Se profiles from SIMS are similar or overlap, indicating the implanted Se ions are embedded in nearly the same depths in the glassy carbon samples implanted at RT and 200 ºC. These results are contrary to the results reported for other elements such as Cs (at 350 and 600 °C) [22] and Cd (430 and 600 °C) [6]. However, radiation enhanced diffusion was not observed for the GC sample implanted at 200 °C. The absence of such diffusion is understandable considering the lower implantation temperature of 200 °C compared to those of Cs and Cd. The experimental R_p values (of both room temperature and 200 °C) agree reasonably with the SRIM simulated value of 132.80 nm, within 5% uncertainties of the SRIM program (see Table 1). The experimental projected range straggling (ΔR_p) values are higher than the SRIM value by 13 and 17% in the RT and 200 °C GC implanted samples. Larger projected range straggling could point to the diffusion of implanted species during implantation [26], but such did not occur in this study. Larger experimental projected range straggling can also be linked to the nanopores present in GC [26]; hence, the discrepancies between the experimental and the calculated projected range straggling. Also reported in Table 1 are the skewness (γ) and kurtosis (β) values. The as-implanted values of γ ranged between 0.28 and 0.29, while β ranged between 2.94 and 2.95. These values are close to $\gamma = 0$ and $\beta = 3$ for an ideal Gaussian distribution; it follows that the SIMS as-implanted profiles (in Figure 1) are nearly Gaussian.

The dpa curve in Figure 1 shows that some of the implanted Se atoms are in the region with low radiation damage, and most of the Se atoms are concentrated in a region of high radiation damage. The maximum damage (in dpa) is at about 100 nm below the surface, which is less than the projected range of the implanted Se. This implies that more selenium atoms are displaced closer to the surface than the bulk. Consequently, this might lead to a preferred diffusion of selenium towards the surface at lower temperatures.

Figures 2 show the Transmission electron microscopy (TEM) micrographs of pristine glassy carbon (high magnification) and the glassy carbon samples implanted with Se ions at RT and at 200 ºC. The TEM micrograph of the pristine glassy carbon indicates densely packed layered graphitic strands nanostructures surrounded by onion-like features. A similar structure of GC was recently reported by Odutemowo et al. [20]. The onion-like features in the TEM micrograph of the pristine glassy carbon, according to Harris, are similar to defective multi-layered fullerenes [12], implying that glassy carbon contains fullerene constituents. Harris developed a model which explains the fullerenes in glassy carbon are responsible for its low reactivity and impermeability properties [12].

The TEM micrographs of the as-implanted samples depict that Se ion implantation damaged the graphitic strands in the glassy carbon from the surface up to a depth of 159.60 nm and 156.91 nm in the RT and 200 ºC as-implanted GC samples, respectively. Figures 2(e) and (f) illustrate the selected area diffraction patterns (SAD) of pristine GC and samples implanted at RT and 200 °C (d-f). Compared to the GC samples implanted at RT and 200 °C, the pristine GC shows more defined rings, indicating that the pristine sample is more graphitic than the as-implanted samples. The diffraction patterns of the GC samples implanted at RT and 200 °C exhibit diffuse rings, as shown in Figures 2(e) and (f). This would imply that these samples contain fewer graphitic crystallites.

Furthermore, the SAD patterns in Figures 2(e) and (f) reveals that these two as-implanted samples types appear to suggest that the surface layer of the glassy carbon samples was damaged following Se ions implantation. Figures 2(e) and (f) seemed to have no difference, implying that both samples are damaged to the same degree. The TEM micrographs of the RT and 200 °C as-implanted samples confirmed this observation.

Comparing the dpa results in Figure 1 and TEM results in Figure 2, it is evident that the damaged layer of 159.60 nm in the room temperature sample corresponds to about 8.5 dpa in Figure 1, which is greater than the critical dpa of 0.2 [27] required to amorphise glassy carbon.

Hence, the surface layer of the glassy carbon samples was completely amorphised due to Se ions implantation at room temperature.

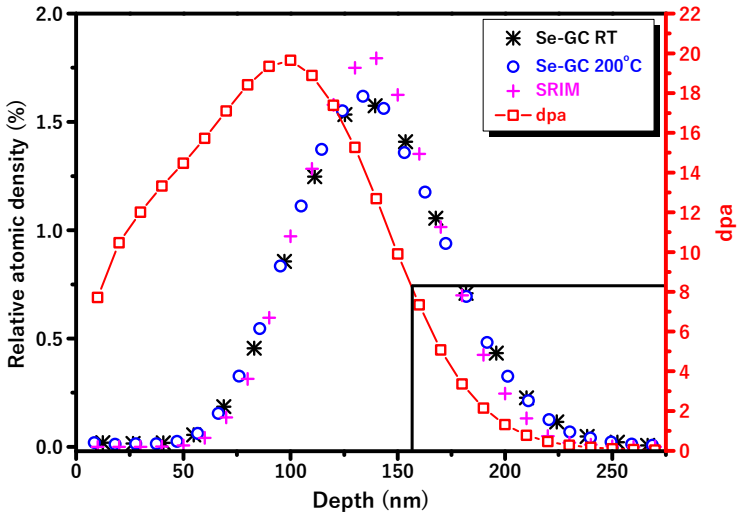

Figure 1. Depth profile of 150 keV Se^+ implanted in GC at RT and 200 ºC. Pink and red lines – ion distributions and dpa from SRIM calculation, black and blue lines – SIMS experiment.

Table 1. The first four moments of Se distribution in glassy carbon. Rp – projected range, ΔRp – projected range straggling, γ - skewness β – kurtosis.

	Simulation	**Experiment**	
Moments	SRIM	RT	200 ºC
$\mathbf{R_p}$	132.80	129.56	130.10
$\mathbf{\Delta R_p}$	30.40	35.40	35.07
$\boldsymbol{\gamma}$	0.18	0.29	0.28
$\boldsymbol{\beta}$	2.86	2.95	2.94

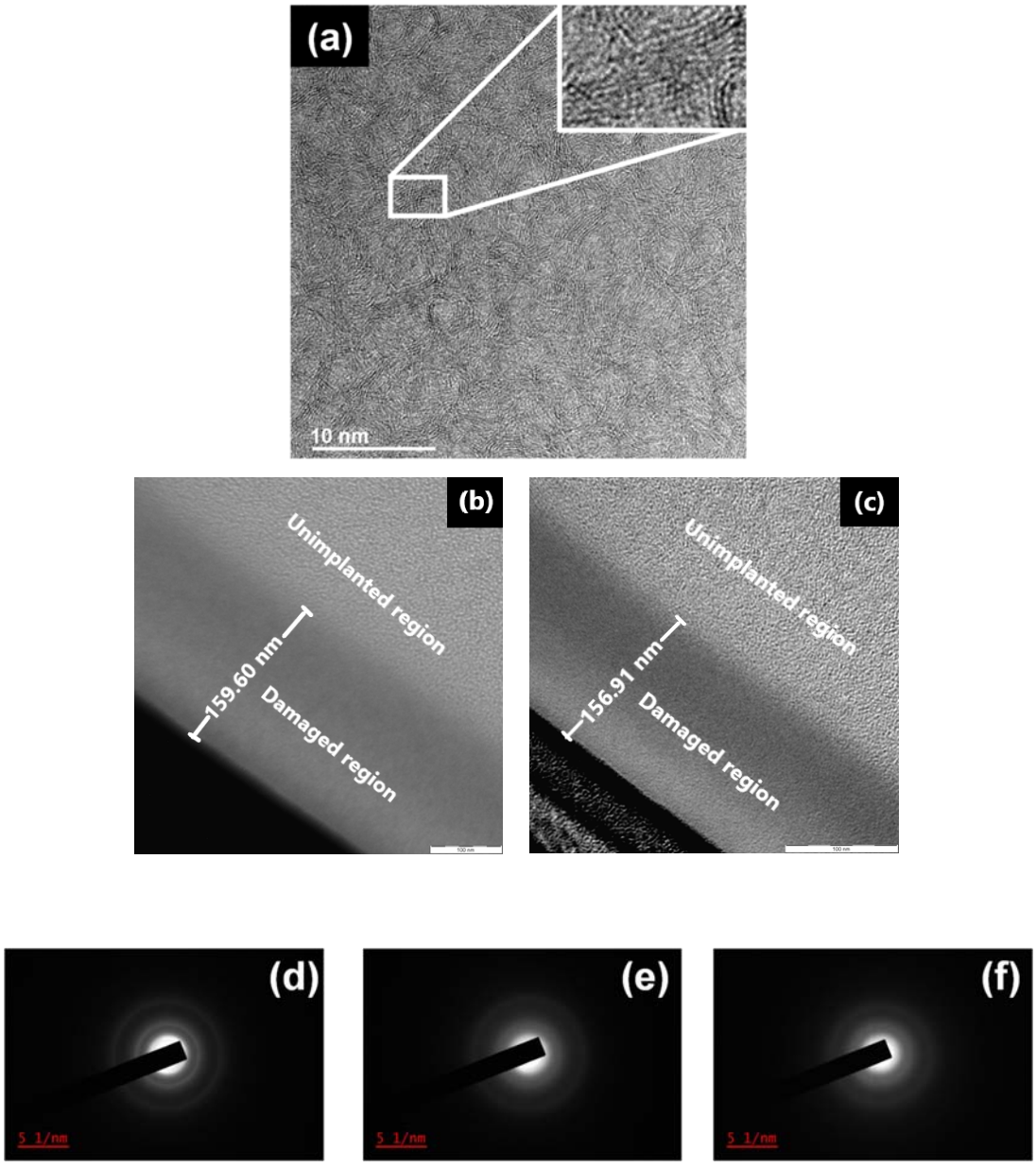

Figure 2. TEM micrographs (high magnification) of (a) The pristine glassy carbon (b) GC implanted at RT and (b) 200 ºC with 150 keV Se ions to 1 × 10 ^{16} cm^{-2}. The selected area diffraction (SAD) patterns of (d) the pristine GC, (e) and (f) implanted region of the GC samples implanted at RT and 200 °C, with 150 keV Se ions to 1 × 10 ^{16} cm^{-2}, respectively.

Figure 3 shows the Raman spectrum of pristine glassy carbon. After the deconvolution of this spectrum, two pronounced peaks were identified at about 1357 cm^{-1} and 1588 cm^{-1}. These pronounced peaks are the D and G peaks, which are characteristic of carbon-based materials with majorly sp^2 bonds and some disorders. The D peak indicates a disordered graphite structure linked to the A_{1g} breathing mode with vibrations near the K zone boundary [28]. The

G peak can be identified as the sp^2 carbon networks in graphite [29]. This peak is due to the Raman optical mode and the E_{2g} symmetry. The peak at ~1170 cm^{-1} is mainly noticed when the acoustic mode is interposed with the optic mode in the vibrational density of the state of carbon materials. The peak at ~1495 cm^{-1} (D'' peak) can be related to the amorphous carbon in the carbon lattice's interstitial sites. The hump around the 1620 cm^{-1} (D') peak is an identity of GC with small-sized crystals.

The Tuinstra-Koenig relation [30] was used to evaluate the average crystallite size in the pristine glassy carbon and the annealed implanted GC samples (see equation (3) below):

$$\frac{ID}{\mathrm{IG}} = \frac{C_\lambda}{L_a} \tag{3}$$

where L_a is the average crystallite size; ID/IG is the D to G peak intensities ratio calculated as 1.67 for the pristine GC. C_λ is the laser excitation wavelength-dependent constant evaluated from the relation, $C_\lambda \approx C_0 + \lambda C_1$ for $400 < \lambda < 700$ nm [31]. C_λ is calculated to be 49.6 Å for λ = 532 nm, C_1 = –126.0 Å, and C_0 = 0.033 estimated from a plot of C_λ versus excitation wavelengths [28]. An average crystallite size of 2.97 nm was calculated for the pristine glassy carbon, which falls in the range, 2.5 nm < L_a < 300 nm, where the Tuinstra-Koening equation holds for different forms of graphitic carbon [28].

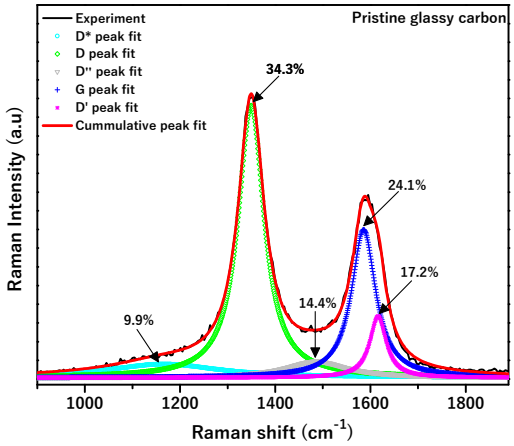

Figure 3. Raman spectrum of pristine glassy carbon. D peak fit (solid cyan line), D peak fit (solid green line), D' peak fit (solid blue line), G peak fit (solid magenta line), D'' peak fit (solid grey line), and the cumulative fit peak (solid red line).*

The implantation of Se ions in GC at room temperature and 200 °C resulted in the disappearance of the characteristic peaks and the appearance of single broad peaks, as shown in Figures 4(a) and 5(a), respectively. The Raman spectra in these Figures are like those of amorphised carbon structures [27,32]. This suggests that the randomly ordered graphitic

microcrystallites in the implanted layer of the GC may have been damaged because of high fluence Se ion implantation. The deconvolution of the Raman spectra of the implanted samples using a Voigt function made it possible to obtain relevant information from parameters such as the G peak position with corresponding FWHM, D to G peak intensities ratio (ID/IG), D to D' peak intensities ratio (ID/ID'), and D'' to G peak intensities ratio (ID''/IG). These parameters are shown in Table 2 and plotted in Figures 6(a-d). The G peak downshifted to 1567 and 1576 cm^{-1} after implantation at RT and 200 °C, respectively, from the initial value of 1588 cm^{-1} for the pristine glassy carbon (see Table (2) and Figure 6(a)).

Furthermore, the G peak FWHM has increased from 59.6 cm (for the pristine glassy carbon) to 147.3 cm for the sample implanted at RT and became narrower to 118.0 cm after implantation at 200 °C, as shown in Table 2 and Figure 6(b). An increase in the FWHM of the G peak (coupled with the downshifting of the G peak positions) after implantation indicates a high level of disorder in the GC and consequent damage of graphitic crystallite, as reported in other studies [7,8,11,20,33]. The higher FWHM value in the RT implanted GC sample indicates a higher level of disorder and damage than the sample implanted at 200°C. As seen in Figures 4(a) and 5(a), the intensities of the convoluted D and G peaks decreased with respect to the implantation temperatures leading to the decrease in the ID/IG ratio from 1.67 (the pristine value) to 1.28 and 1.55 in the RT and 200 °C implanted glassy carbon samples, respectively (see Table 2 and Figure 6(c)).

The merging of the D and G peaks alongside the increase in the FWHM, the decrease in the ID/IG ratio, and the shift of the G peak positions to lower wavenumber were used to rank the degree of disorder in the structures of the implanted glassy carbon samples due to the Se ion bombardment at different implantation temperatures. The structural damage due to Se implantation is greater for the sample implanted at RT compared to the 200 °C Se implanted GC sample. This observation indicates the damage to the implanted GC structures decreases with increasing implantation temperature. A similar trend was observed when Cd ions were implanted in GC at RT, 430, and 600 °C [6]. The Raman spectrum of the room temperature Cd implanted glassy carbon sample is similar to the Raman spectrum of the RT Se implanted GC sample obtained in this study. However, the Raman spectra of the GC samples implanted at 430 and 600 °C have more pronounced D and G peaks, indicating less damage in their substrate's structures compared to the 200 °C glassy carbon substrate in this study. The absence of the D and G peaks in the Raman spectrum of the 200 °C implanted GC glassy carbon is due to more structural damage at this lower implantation temperature.

Typically, a decrease in the ID/IG ratio after implantation may imply smaller graphitic crystallite sizes within the damaged layer of the implanted glassy carbon substrates. The average crystallite sizes within the damaged layer after implantation were estimated using the relation by Ferrari and Robertson [28]. The Ferrari-Robertson relation in equation (4) is more appropriate for amorphous and carbon materials with crystallite sizes less than 2.5 nm [28]. An explanation to justify why equation (4) was given in our article in Ref. [8].

$$\frac{\mathrm{ID}}{\mathrm{IG}} = C_{\lambda}' L_a^2 \quad (4)$$

where C_{λ}' is a constant given as 0.0055 Å^{-2} [29], and L_a is the average crystallite size. The amorphisation of the implanted layer in the GC resulted in smaller crystallite sizes, 1.53 and 1.68 nm after implantation at RT and 200 °C, respectively (see Table 2 and Figure 6(c). This result confirms that the implantation of Se ions in glassy carbon leads to the damage of the graphitic strands embedded in the glassy carbon and leaves the substrate with disordered layers characterised with average smaller crystallite sizes. The slightly larger crystallite size in the 200 °C implanted glassy carbon indicates less structural damage compared to the RT implanted GC sample.

The ID''/IG ratio represents the ratio of amorphous carbon (D'') relative to the graphitic carbon (G) in the GC samples [34]. It can be seen in Figure 6(d) that the ID''/IG ratio is 0.10 for the pristine GC and increased to 1.04 and 1.10 after implantation with Se ions at RT and 200 °C, respectively. The increase in the ID''/IG ratio further confirms that the GC becomes defective after high fluence Se ion implantation. The defects in the implanted GC samples were identified using the ID/ID' ratio parameter. Eckmann et al. [35] have used ID/ID' to characterise the defects in Ar^+ bombarded graphenes, hydrogenated and fluorinated graphites. The authors reported sp^3 defect type for ID/ID' ≃ 13; vacancy-like defects for ID/ID' ≃ 7; and boundary-like defects for ID/ID' ≃ 3.5. In another study by Madito et al. [34], the ID/ID' ratio was used to characterise the defects in GC samples implanted with Xe ions. The authors justified the defects characterisation in the GC, which was the presence of randomly oriented graphitic strands embedded within its structure [34]. In this study, a similar defect characterisation was carried out using the ID/ID' ratio. The ID/ID' ratio in the pristine GC was calculated to be 5.92, indicating a boundary-like defect in this structure. The ID/ID' ratio decreased to 1.87 and 2.04 after the implantation of Se ions into GC at RT and 200 °C, respectively indicating the reduction of the boundary defect in the implanted GC. A similar reduction in boundary defect was reported in GC implanted with 200 keV Xe ions at RT [34].

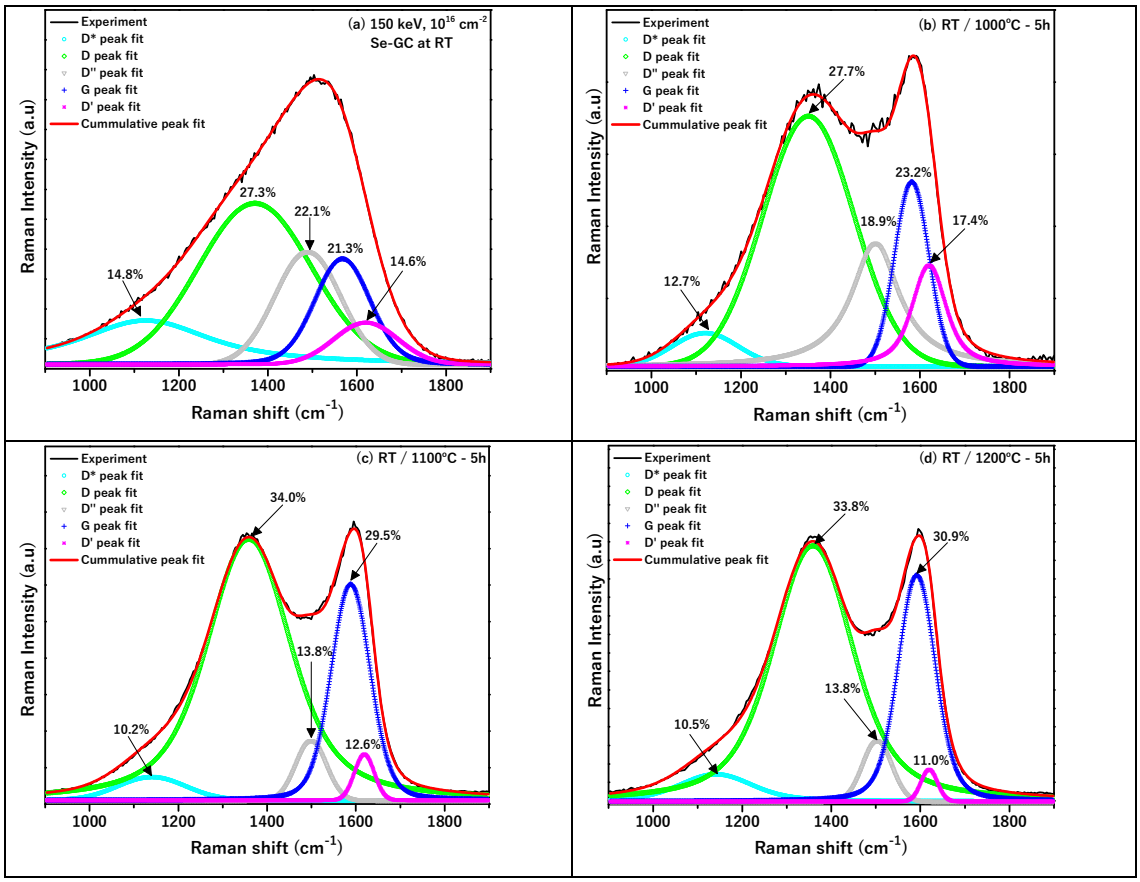

Figure 4. Raman spectra of Se implanted in glassy carbon (a) at room temperature and after annealing for 5 h in vacuum at (b) 1000 °C (c) 1100 °C (d) 1200 °C.

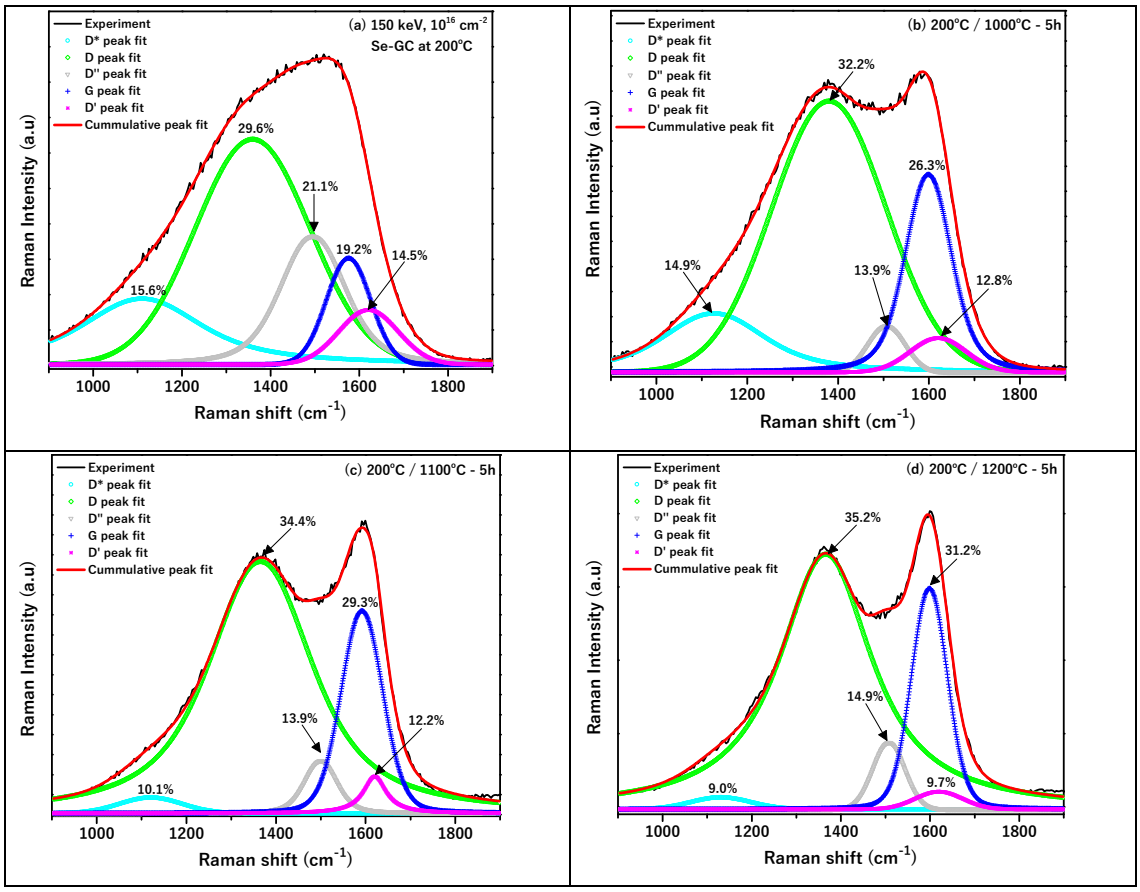

Figure 5. Raman spectra of Se implanted in glassy carbon (a) at 200 °C, and after annealing for 5 h in vacuum at (b) 1000 °C (c) 1100 °C (d) 1200 °C.

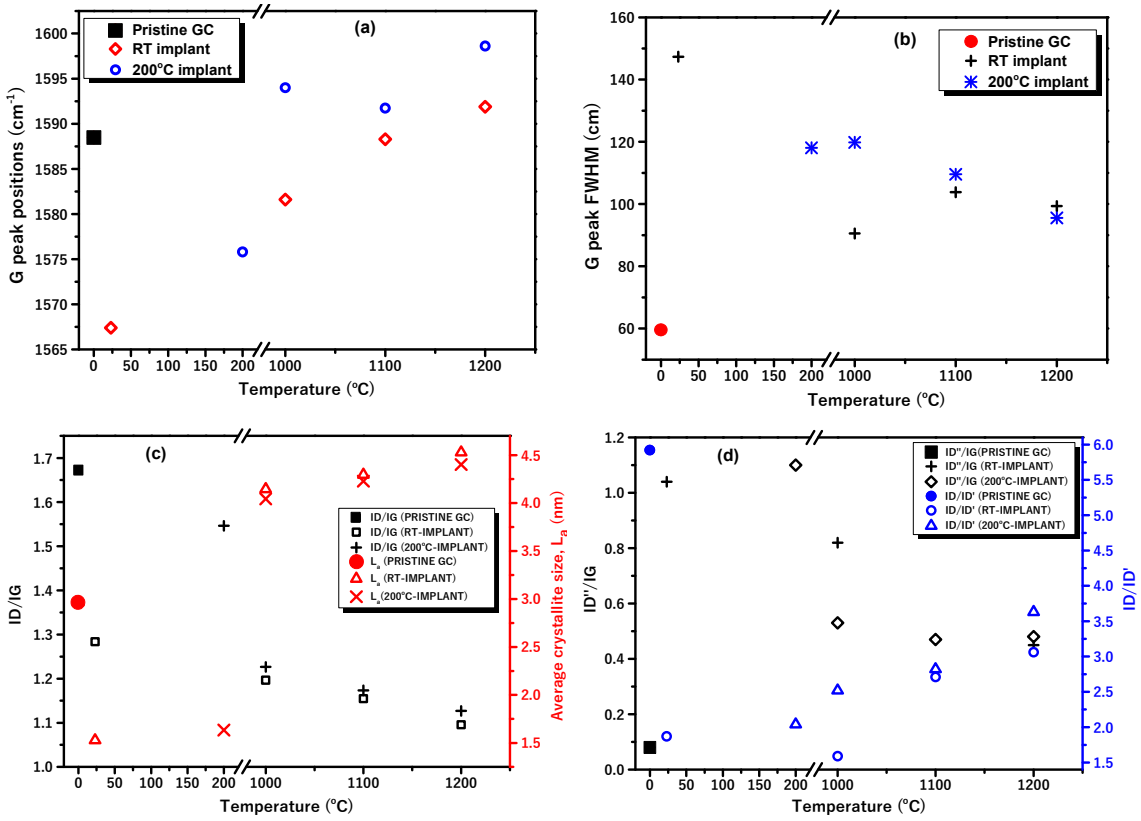

Figure 6. Raman fitting parameters (a) G peak positions (cm^{-1}) (b) G peak FWHM (c) ID/IG ratio and L_a (nm) (d) ID''/IG ratio and ID/ID' ratio, of the acquired Raman spectra of glassy carbon implanted with 150 keV Se ions at room temperature and 200 °C after isochronally annealed at 1000, 1100, and 1200 for 5h.

Table 2. The Raman results for 150 keV Se ions implanted in glassy carbon at room temperature and 200°C and after sequential isochronally annealed at 1000, 1100, and 1200°C for 5h. All spectra compared with the pristine glassy carbon. RT/AS – Se implanted glassy carbon at room temperature; 200/AS – Se implanted glassy carbon at 200 °C; RT/1000 – Se implanted glassy carbon at room temperature and annealed at 1000 °C; 200 /1000 – Se implanted glassy carbon at 200 °C and annealed at 1000 °C

Sample tag	G-peak position	G-peak FWHM	ID/IG	La (nm)	ID''/IG	ID/ID'
Pristine GC	1588.5	59.6	1.67	2.97	0.10	5.92
RT-AS	1567.4	147.3	1.28	1.53	1.04	1.87
RT/1000	1581.6	90.53	1.20	4.15	0.82	1.59
RT/1100	1588.3	103.8	1.15	4.30	0.47	2.71
RT/1200	1591.9	99.3	1.10	4.53	0.45	3.06
200/AS	1575.8	118.0	1.55	1.68	1.10	2.04
200/1000	1594.0	119.8	1.23	4.04	0.53	2.52
200/1100	1591.7	109.6	1.17	4.23	0.47	2.82
200/1200	1598.6	95.5	1.13	4.40	0.48	3.63

The effect of annealing on the structure of the GC samples implanted at RT and 200 °C with 150 keV Se ions was studied by Raman spectroscopy. Annealing the samples at 1000, 1100, and 1200 °C for 5 h (under vacuum) caused a change in the Raman spectra, as shown in Figures 4(b-d) & 5(b-d). The D and G peaks reappeared after annealing at 1000 °C and became enhanced after annealing at 1100 and 1200 °C. The progressive growth of the D and G peak intensities would imply that the implantation damage was being annealed out and consequently an increase in the graphitic order of the GC substrates. This is confirmed by the behaviour of the peak parameters (see Table 2 and Figures 6(a-d)) after deconvolution, discussed in the next paragraph.

The G peak position shifted to higher wavenumbers after isochronal annealing the GC samples initially implanted with Se ions at RT and 200 °C. After annealing at 1200 °C, the G peak positions upshifted to 1592 and 1599 cm^{-1}, respectively, as shown in Table 2 and Figure 6(a). It can also be seen in Table 2 and Figure 6(b) that annealing caused the G peak FWHM values of the RT and the 200 °C GC samples to become smaller than the as-implanted ones but still larger than the pristine GC. In addition, a progressive decrease in the ID/IG ratio was observed for the RT and 200 °C GC samples after annealing between 1000 °C and 1200 °C. Typically annealing would result in the recrystallisation within the implanted layer of the GC substrates. The recrystallisation due to annealing was checked by calculating the average crystallite sizes using equation (3). The crystallite sizes (of the GC substrates) have increased from 4.15 to 4.53 nm and 4.04 to 4.40 nm after annealing the room temperature and 200 °C as-implanted GC samples, respectively in the same temperature range (i.e., 1000 – 1200 °C). The enhanced G peak intensities in the structures of the annealed GC samples would justify the increased larger crystallite sizes.

The changes in the G peak positions and FWHM, ID/IG, and L_a are evidence of structural recovery in the as-implanted samples after annealing. However, it was necessary to note that the final structures of all the annealed implanted samples are not the same as the pristine GC even after annealing at the highest temperature of 1200 °C. Thus, some radiation damage was retained in the GC substrates. Impurity retainment within the GC structure may have inhibited the complete structural recovery of the GC substrates. Other studies have shown that heat treatment of ions implanted in GC samples does not usually remove all radiation damage due to retained defects [5–8,32]. As shown in Figure 6(d), the ID'/IG ratio values of the ID''/IG ratio reduced to values lower than the as-implanted ones but higher than the pristine value. This observation indicates the reduction of the amorphous carbon fraction within the implanted region of the annealed samples. Annealing increased the ID/ID' ratio to a values

close to the pristine value indicating structural recovery and re-emerging of the boundary-like defect in the glassy carbon substrates. The changes reported for ID'/IG and ID/ID' ratios further point to the recovery of the GC substrates after annealing.

Using the secondary ion mass spectrometry technique, the effects of annealing on Se distribution in the temperature range of 1000 – 1200 °C (in steps of 100 °C for 5h) were investigated. Figures 7(a) and (b) show Se's depth profiles implanted into GC samples at RT and 200 °C both before and after annealing. The selenium retained ratio plotted as a function of annealing temperatures is also shown in Figure 7(c). The retained ratio was calculated as the ratio of the area of the Se profile (i.e., the Se concentration) after each annealing temperature to that of the as-implanted ones.

The isochronal annealing of the room temperature implanted sample at 1000 °C resulted in the asymmetric broadening of the Se profile, as shown in Figure 7(a). The 1000 °C annealed Se profile was skewed to a depth of about 300 nm. The skewness of this profile is an indication of Se atoms' migration into the bulk of the GC. No loss of Se was recorded at this temperature since no migration towards the surface was observed. Increasing the annealing temperature to 1100 °C resulted in an enhanced asymmetrical broadening of the Se profile to the surface and tailing towards the bulk, up to ~325 nm. The Se profile at this temperature implies more Se atoms have migrated into the bulk of the glassy carbon and the surface region, accompanied by about a 36 % loss of Se atoms. The loss of Se can be related to the evaporation of Se atoms into the vacuum during annealing. The melting point of Se being 220 °C is significantly less than the annealing temperatures (1000 – 1200 °C). A similar profile, like the one obtained at 1100 °C, was obtained after annealing the room temperature implanted sample at 1200 °C, indicating a similar migration behaviour of the Se atoms. The tail of the Se profile at this temperature was deeper at a depth of about 400 nm (indicating a stronger migration of Se into the bulk), accompanied by the loss of more Se atoms (of about 51 %).

Annealing the 200 °C GC sample at 1000 °C resulted in an asymmetric Se profile with an appearance of a smaller peak at a depth of about 30 nm below the surface. This asymmetric profile tailed towards the bulk up to a depth of 350 nm, as shown in Figure 7(b). The smaller surface peak indicates the accumulation of Se atoms (i.e., segregation) at the surface, accompanied by a loss of about 10 %. The tailing of the profile suggests that some Se atoms have migrated into the bulk matrix of the GC. After annealing the 200 °C GC implants at 1100 and 1200 °C, the surface peaks became pronounced, indicating more Se atoms segregated towards the surface. However, a significant loss of about 31 % and 40 % Se atoms was observed after annealing these 200 °C GC implants at 1100 and 1200 °C, respectively. Accompanying

the surface segregation is the migration of Se atoms deeper into the bulk of the GC, up to a maximum depth of ~ 400 nm.

The Se atoms exhibit a similar migration behaviour into the bulk of both RT and 200 °C implanted samples. By referring to the dpa curve included in Figures 7(a) and (b), it can be seen that the radiation damage is lower at the end of range region (i.e., at 240 nm) as compared to the rest of the implantation layer. Accordingly, the migration of the Se atoms is not expected in the bulk since much of the radiation damage (~ 19 dpa was at a depth of 100 nm) is closer to the surface than the bulk of the GC substrates. But it can be seen from Figures 7(a) and (b) that the migration of Se atoms started from the region with the minimum damage and progressed to moderate and high radiation damage region with respect to increasing annealing temperature. This type of migration behaviour exhibited by the Se atoms in the bulk of both RT and 200 °C implants (after annealing) can be explained in terms of trapping and de-trapping of the Se atoms by defects induced at implantation. The migration of the Se atoms deeper into the bulk (of the annealed samples) occurred as a result of defect annealing in the less radiation damage region. However, the trapping of the majority of the Se atoms in the high radiation damage region restricted its migration towards the surface, especially in the RT implanted sample. The Pristine GC contains several nanopores, accounting for its low density (1.42 gcm^{-3}). Since the average pore size in GC is about 0.3 nm [36], then a Se atom with an atomic radius of 0.19 nm would successfully fit into a pore of 0.3 nm size. Consequently, the irradiated glassy carbon would have fewer micropores and the Se atoms trapped by the irradiation defects [20]. The RT and 200°C Se experimental depth profiles are further indications that Se atoms are trapped as these profiles are slightly broader than the simulation (see Figure 1 and ΔR_p in Table 1).

The migration of Se atoms towards the surface in the annealed RT and 200 °C as-implanted samples occurred after the radiation damage had been annealed out. Notably, the migration behaviour of the Se atoms towards the surface in both sample types (after annealing) is different despite showing similar ion distribution at implantation and subjecting them to isochronal annealing in the same temperature range (i.e., 1000 – 1200 °C). For example, the migration of Se atoms towards the surface occurred after annealing the RT as-implanted sample at 1100 °C. In contrast, migration of the Se atoms towards the surface in the 200 °C as-implanted sample starts at 1000 °C. In addition, the humps in Figure 7(b) indicates the segregation of the Se atoms towards the surface of the 200 °C as-implanted samples after annealing from 1000 °C up to 1200 °C. Figure 7(a) shows that no such segregation occurred after annealing the RT as-implanted samples in the same temperature range. These differences

in the migration behaviour of Se atoms towards the surface of the RT and 200 °C as-implanted samples (after annealing) suggest the initial effect of ion implantation on the GC substrates. Typically, radiation damage depends on the implantation temperatures and due to dynamic annealing, more damage is expected for RT implantation than that performed at higher temperatures. Transmission electron microscopy (TEM) and Raman spectroscopy are two essential techniques to investigate radiation damage evolution and structural changes in ion-bombarded materials. It can be recalled from Figures 4(a) and 5(a) that the Raman spectra of the RT and the 200 °C GC as-implanted samples are different. Less structural damage was observed in the 200 °C as-implanted samples than in the RT sample. In addition, the magnitude of radiation damage in the room temperature as-implanted sample is more than the 200 °C as-implanted samples (as shown in the diffraction patterns inserted in the TEM images in Figures 2(a) and (b)). The different migration behaviour of Se atoms toward the surface in both annealed as-implanted glassy carbon samples can be related to the trapping and de-trapping of the Se atoms in different amounts of ion-induced defects in the two samples. An example can be seen in Figure 7(c), where the retained Se impurities in the sample implanted at 200 °C and annealed at 1200 °C are more than those in the RT sample annealed at the same temperature.

The migration behaviour of Se in glassy carbon compared with other previous fission elements studied [22,23,33] does not show a similar migration pattern (by the depth profiles) despite the segregation and bulk migration exhibited by these elements. Two probable explanations can be given for the variation mentioned above in the migration pattern of Se and other fission elements. The first is the possibility of the synergistic effect of an array of fission elements in the host nuclear waste. The radioactivity of a nuclear waste gives rise to many fission elements and these fission elements can coexist together, giving rise to the synergistic effect between them. Another reason could be the differences in the microstructures of the as-implanted glassy carbon after annealing, which otherwise affected the migration behaviour of the initially implanted fission elements.

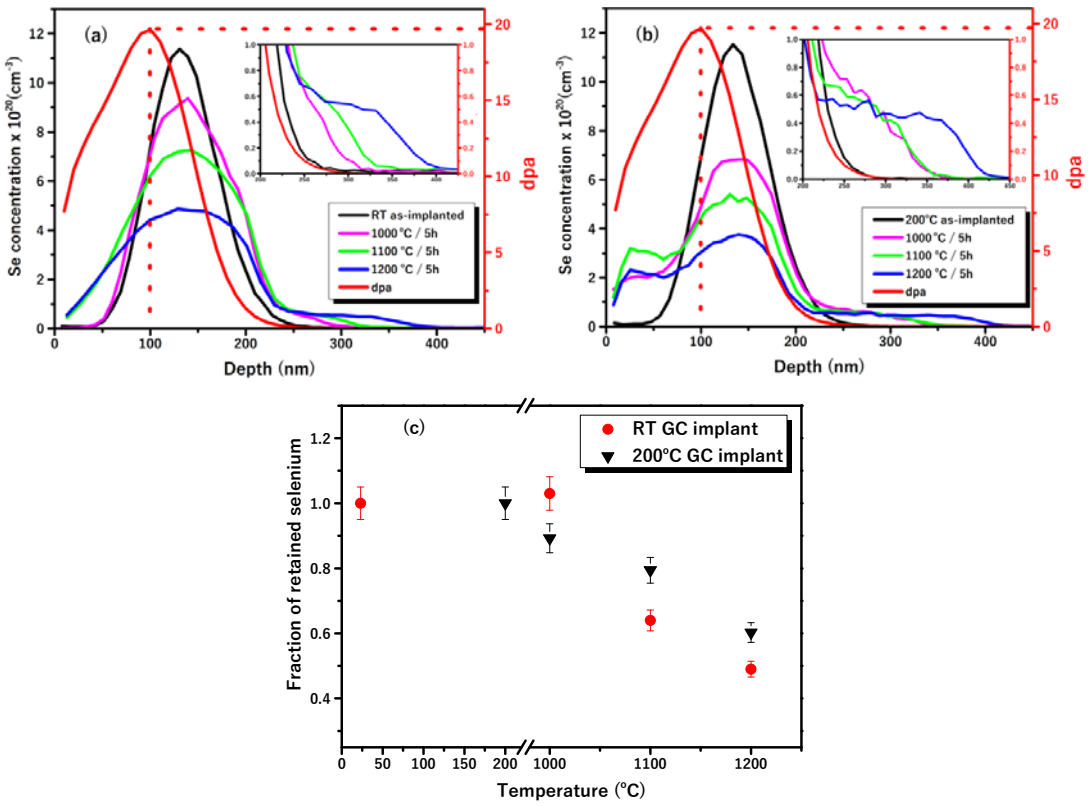

Figure 7. SIMS depth profiles of 150 keV Se ions implanted in glassy carbon at (a) RT and (b) 200 °C (c) fraction of retained Se in the glassy carbon substrate after annealing the RT and 200 °C implanted samples at 1000, 1100, and 1200 °C for 5h in steps of 100 °C.

4. Conclusions

In the present work, GC samples were implanted with 150 keV Se ions at room temperature (RT) and 200 ºC to a fluence of 1×10^{16} ions/cm^2. The effects of implantation temperatures and isochronal vacuum annealing on the structural evolution and migration of Se implanted into glassy carbon (GC) were investigated by a combination of Transmission electron microscopy (TEM), Raman spectroscopy and secondary ion mass spectrometry (SIMS). The TEM and Raman results show that the Se implantation induces damage at nearly similar depth in the as-implanted room temperature and 200 ºC GC substrates. Similarly, the structure of the GC samples was damaged by Se ions implantation, with more defects observed in the RT implanted sample. Annealing caused gradual defect removal in both sample types accompanied by a reduction in the amorphous carbon fraction within the implanted region of the annealed samples. However, the structure of the as-implanted glassy carbon samples has not fully recovered even after annealing at the highest temperature used (1200 ºC). According

to the Raman analysis result, boundary-like defects exist in the as-implanted GC samples and are retained after annealing both sample types up to 1200 ºC.

The results also indicate the minor role of the implantation temperature on the depth profiles of Se atoms. Moreover, the Se atoms exhibited a similar migration into the bulk of the room temperature and the 200 ºC implanted samples after annealing at 1000 ºC. However, a different migration behaviour of the Se atoms towards the surface was observed for the RT and the 200 ºC implanted samples after annealing at 1000 – 1200 ºC. For instance, in contrast to the RT implanted sample, the Se atoms were segregated on the surface of the 200 ºC implanted sample. The different migration behaviour in the samples implanted at different temperatures is attributed to the interaction of the Se atoms with ion-induced defects. After annealing at 1200 ºC, more Se atoms were retained in the 200 ºC implanted sample than the RT one. This relates again to the sample's microstructure after implantation, leading to the enhanced Se segregation in the annealed 200 ºC implanted sample. Segregation would prevent the loss of Se atoms at the surface of the 200 ºC implanted sample. Despite that the diffusion of Se into the bulk of the glassy carbon substrates is not efficient, the concentration of the Se atoms migrating to the surface is much higher than that migrated into the bulk. The results of this study could point to the need to improve the glassy carbon for its application as a potential storage material for radioactive nuclear wastes. However, the influence of other fission products elements on the migration of Se must be studied before proposing any recommendation for the improvement of glassy carbon for nuclear waste storage application.

Acknowledgement

Special thanks to Prof. Elke Wendler and her technical team at the Institut für Festkörperphysik, Friedrich-Schiller-Universit¨at Jena, Germany, assisted during parts of the experiment that made this work a success. Adeojo Samuel Adedigba appreciates the AST&D scholarship from the Tertiary Education Trust Fund (TETFund), Nigeria, and the Postgraduate Bursary from the University of Pretoria, South Africa. The Research Council of Norway is acknowledged for the support to the Norwegian Micro- and Nano-Fabrication Facility, NorFab, project number 295864.

References

[1] A. Erhard, H. Völzke, U. Probst, D. Wolff, Aging management for long-term interim storage casks, Packag. Transp. Storage Secur. Radioact. Mater. 22 (2011) 46–53. https://doi.org/10.1179/1746510910y.0000000013.

[2] J.B. Malherbe, O.S. Odutemowo, E.G. Njoroge, D.F. Langa, T.T. Hlatshwayo, C.C. Theron, Ion bombardment of glassy carbon, Vacuum. 149 (2018) 19–22. https://doi.org/10.1016/j.vacuum.2017.11.006.

[3] O.S. Odutemowo, J.B. Malherbe, L. Prinsloo, D.F. Langa, E. Wendler, High temperature annealing studies of strontium ion implanted glassy carbon, Nucl. Instruments Methods Phys. Res. Sect. B Beam Interact. with Mater. Atoms. 371 (2016) 332–335. https://doi.org/10.1016/j.nimb.2015.10.054.

[4] O.S. Odutemowo, M.S. Dhlamini, E. Wendler, D.F. Langa, M.Y.A. Ismail, J.B. Malherbe, Effect of heat treatment on the migration behaviour of Sr and Ag CO-implanted in glassy carbon, Vacuum. 171 (2020) 109027. https://doi.org/10.1016/j.vacuum.2019.109027.

[5] M.Y.A. Ismail, J.B. Malherbe, O.S. Odutemowo, E.G. Njoroge, T.T. Hlatshwayo, M. Mlambo, E. Wendler, Investigating the effect of heat treatment on the diffusion behaviour of xenon implanted in glassy carbon, Vacuum. 149 (2018) 74–78. https://doi.org/10.1016/j.vacuum.2017.12.021.

[6] T.T. Hlatshwayo, L.D. Sebitla, E.G. Njoroge, M. Mlambo, J.B. Malherbe, Annealing effects on the migration of ion-implanted cadmium in glassy carbon, Nucl. Instruments Methods Phys. Res. Sect. B Beam Interact. with Mater. Atoms. 395 (2017) 34–38. https://doi.org/10.1016/j.nimb.2017.01.086.

[7] E.G. Njoroge, L.D. Sebitla, C.C. Theron, M. Mlambo, T.T. Hlatshwayo, O.S. Odutemowo, V.A. Skuratov, E. Wendler, J.B. Malherbe, Structural modification of indium implanted glassy carbon by thermal annealing and SHI irradiation, Vacuum. 144 (2017) 63–71. https://doi.org/10.1016/j.vacuum.2017.07.020.

[8] S.A. Adeojo, J.B. Malherbe, E.G. Njoroge, M. Mlambo, O.S. Odutemowo, T.T. Thabethe, Z.A.Y. Abdalla, T.T. Hlatshwayo, Effect of sequential isochronal annealing on the structure and migration behaviour of selenium-ion implanted in glassy carbon, Vacuum. 182 (2020) 109689. https://doi.org/10.1016/j.vacuum.2020.109689.

[9] A.J. Innocent, T.T. Hlatshwayo, E.G. Njoroge, J.B. Malherbe, Interface interaction of tungsten film deposited on glassy carbon under vacuum annealing, Vacuum. 148

(2018) 113–116. https://doi.org/10.1016/j.vacuum.2017.11.020.

[10] A.J. Innocent, T.T. Hlatshwayo, E.G. Njoroge, T.P. Ntsoane, M. Madhuku, E.O. Ejeh, M. Mlambo, M.Y.A. Ismail, C.C. Theron, J.B. Malherbe, Evaluation of diffusion parameters and phase formation between tungsten films and glassy carbon, Vacuum. 175 (2020) 109245. https://doi.org/10.1016/j.vacuum.2020.109245.

[11] E.G. Njoroge, T.T. Hlatshwayo, M. Mlambo, O. Odutemowo, K.A. Annan, A. Skuratov, M. Ismail, J.B. Malherbe, Nuclear Inst . and Methods in Physics Research , B Effect of thermal annealing on SHI irradiated indium implanted glassy carbon, Nucl. Inst. Methods Phys. Res. B. 502 (2021) 66–72. https://doi.org/10.1016/j.nimb.2021.06.011.

[12] P.J.F. Harris, Fullerene-related structure of commercial glassy carbons, Philos. Mag. 84 (2004) 3159–3167. https://doi.org/10.1080/14786430410001720363.

[13] P.J.F. Harris, New perspectives on the structure of graphitic carbons, Crit. Rev. Solid State Mater. Sci. 30 (2005) 235–253. https://doi.org/10.1080/10408430500406265.

[14] P.J.F. Harris, S.C. Tsang, High-resolution electron microscopy studies of non-graphitizing carbons, Philos. Mag. A Phys. Condens. Matter, Struct. Defects Mech. Prop. 76 (1997) 667–677. https://doi.org/10.1080/01418619708214028.

[15] S.S. Bukalov, L.A. Leites, A.I. Sorokin, A.S. Kotosonov, Structural changes in industrial glassy carbon as a function of heat treatment temperature according to Raman spectroscopy and X-ray diffraction data, Nano: Phys., Chem., Math. 5 (2014) 186–191.

[16] A.L. Nichols, D.L. Aldama, M. Valleti, Handbook of Nuclear Data for Safeguards, IAEA Nuclear Data Section, INDC (NDS)-0502, Vienna, Austria, 2007, pp. 1–94.

[17] G. Shaw, D. Ashworth, Selenium: Radionuclides, Encycl. Inorg. Chem. (2010). https://doi.org/10.1002/0470862106.ia718.

[18] J. Gerhard, S. Hollas, N. Kivel, K. Kossert, S. Van Winckel, C. Lierse, Preparation of radiochemically pure ^{79}Se and highly precise determination of its half-life, J. Appl. Rad. Isot. 68 (2010) 2339–2351, https://doi.org/10.1016/j.apradiso.2010.05.006.

[19] J. Peterson, M. MacDonell, L. Haroun, F. Monette, R.D. Hildebrand, A. Taboas, Radiological and Chemical Fact Sheets to Support Health Risk Analyses for Contaminated Areas, Argonne National Lab, EVS, 2005, pp. 1–133. http://ww. nuceng.ca/refer/radiation/anl-factsheets.pdf%5Cnpapers2://publication/uuid /4ABDB82D-0580-4E66-A891-DFBF74A7FA94.

[20] O.S. Odutemowo, J.B. Malherbe, L.C. Prinsloo, E.G. Njoroge, R. Erasmus, E.

Wendler, A. Undisz, M. Rettenmayr, Structural and surface changes in glassy carbon due to strontium implantation and heat treatment, J. Nucl. Mater. 498 (2018) 103–116. https://doi.org/10.1016/j.jnucmat.2017.10.018.

[21] O. Koskelo, U. Köster, I. Riihimäki, J. Räisänen, Migration kinetics of ion-implanted beryllium in glassy carbon, Diam. Relat. Mater. 17 (2008) 1991–1993. https://doi.org/10.1016/j.diamond.2008.06.002.

[22] D.F. Langa, N.G. Van Der Berg, E. Friedland, J.B. Malherbe, A.J. Botha, P. Chakraborty, E. Wendler, W. Wesch, Heat treatment of glassy carbon implanted with cesium at room and high temperatures, Nucl. Instruments Methods Phys. Res. Sect. B Beam Interact. with Mater. Atoms. 273 (2012) 68–71. https://doi.org/10.1016/j.nimb.2011.07.041.

[23] O.S. Odutemowo, J.B. Malherbe, C.C. Theron, E.G. Njoroge, E. Wendler, In-situ RBS studies of strontium implanted glassy carbon, Vacuum. 126 (2016) 101–105. https://doi.org/10.1016/j.vacuum.2016.01.024.

[24] Hochtemperatur-werkstoffe GmbH, Germany, properties of glassy carbon. http:// www.htw-germany.com/technology.php5?lang=en&nav0=2. (Accessed 19 February 2020).

[25] T. Hlatshwayo, Diffusion of silver in 6H-SiC, University of Pretoria, Pretoria, South Africa., 2010. http://upetd.up.ac.za/thesis/available/etd-06182011-165556/.

[26] J.B. Malherbe, O.S. Odutemowo, C.C. Theron, E. Wendler, I. Festkörperphysik, F. Jena, Diffusion of strontium implanted in glassy carbon, (2021).

[27] D.G. McCulloch, S. Prawer, A. Hoffman, Structural investigation of xenon-ion-beam-irradiated glassy carbon, Phys. Rev. B. 50 (1994) 5905–5917. https://doi.org/10.1103/PhysRevB.50.5905.

[28] A.C. Ferrari, J. Robertson, Interpretation of Raman spectra of disordered and amorphous carbon, Phys. Rev. B 61 (2000) 14095–14107, https://doi.org/ 10.1136/ip.2010.029215.730.

[29] M.A. Pimenta, G. Dresselhaus, M.S. Dresselhaus, L.G. Cançado, A. Jorio, R. Saito, Studying disorder in graphite-based systems by Raman spectroscopy, Phys. Chem. Chem. Phys. 9 (2007) 1276–1291. https://doi.org/10.1039/b613962k.

[30] F. Tuinstra, J.L. Koenig, Raman Spectrum of Graphite, J. Chem. Phys. 53 (1970) 1126–1130. https://doi.org/10.1063/1.1674108.

[31] M.J. Matthews, M.A. Pimenta, G. Dresselhaus, M.S. Dresselhaus, M. Endo, Origin of dispersive effects of the raman d band in carbon materials, Phys. Rev. B - Condens.

Matter Mater. Phys. 59 (1999) R6585–R6588. https://doi.org/10.1103/PhysRevB.59.R6585.

[32] D.G. McCulloch, S. Prawer, The effect of annealing and implantation temperature on the structure of C ion - beam - irradiated glassy carbon, J. Appl. Phys. 78 (1995) 3040–3047. https://doi.org/10.1063/1.360054.

[33] M.Y.A. Ismail, Z.A.Y. Abdalla, E.G. Njoroge, O.S. Odutemowo, T.T. Hlatshwayo, Nuclear Inst . and Methods in Physics Research , B Effect of high temperature annealing and SHI irradiation on the migration behaviour of Xe implanted into glassy carbon, Nucl. Inst. Methods Phys. Res. B. 489 (2021) 11–19. https://doi.org/10.1016/j.nimb.2020.12.012.

[34] M.J. Madito, M.Y.A. Ismail, T.T. Hlatshwayo, C.B. Mtshali, Applied Surface Science The nature of surface defects in Xe ion-implanted glassy carbon annealed at high temperatures : Raman spectroscopy analysis, Appl. Surf. Sci. 506 (2020) 145001. https://doi.org/10.1016/j.apsusc.2019.145001.

[35] A. Eckmann, A. Felten, A. Mishchenko, L. Britnell, R. Krupke, K.S. Novoselov, C. Casiraghi, Probing the Nature of Defects in Graphene by Raman Spectroscopy, (2012).

[36] H.O. Pierson, Handbook of carbon, graphite, diamond and fullerenes: properties, processing and applications, Noyes Publications, New Jersey, (1993).